Author(s): Torvinen, Katariina; Pettersson, Fredrik; Lahtinen, Panu; Arstila, Kai; Kumar, Vinay; Osterbacka, Ronald; Toivakka, Martti; Saarinen, Jarkko J

Title: Nanoporous kaolin – cellulose nanofibril composites for printed electronics

Year: 2017

Version:

Please cite the original version:

Torvinen, K., Pettersson, F., Lahtinen, P., Arstila, K., Kumar, V., Osterbacka, R., Toivakka, M., & Saarinen, J. J. (2017). Nanoporous kaolin – cellulose nanofibril composites for printed electronics. Flexible and Printed Electronics, 2(2), Article 024004. https://doi.org/10.1088/2058-8585/aa6d97

Nanoporous kaolin – cellulose nanofibril composites for printed electronics

Nanoporous kaolin – cellulose nanofibril composites for printed electronics

Katariina Torvinen[1], Fredrik Pettersson[2], Panu Lahtinen[3], Kai Arstila[4], Vinay Kumar[5], Ronald Österbacka[2], Martti Toivakka[5] and Jarkko J. Saarinen[5]

[1]VTT Technical Research Centre of Finland Ltd, P.O Box 1603, FI-40101 Jyväskylä, Finland

[2] Physics and Center for Functional materials, Åbo Akademi University, Porthansgatan 3, FI-20500 Åbo/Turku, Finland

[3] VTT Technical Research Centre of Finland Ltd, P.O. Box 1000, FI-02044 VTT Espoo, Finland

[4] University of Jyväskylä, Physics Department FI-40014 University of Jyväskylä, Finland

[5] Laboratory of Paper Coating and Converting for Functional materials, Åbo Akademi University, Porthansgatan 3, FI-20500 Åbo/Turku, Finland

Corresponding author:

Katariina Torvinen, M.Sc.

VTT Technical Research Centre of Finland, P.O Box 1603, FI-40101 Jyväskylä, Finland

e-mail: Katariina.Torvinen@vtt.fi, +358 (0) 40 197 3533

Abstract

Cellulose nano- and microfibrils (CNF/CMF) grades vary significantly based on the raw materials and process treatments used. In this study four different CNF/CMF grades were combined with kaolin clay pigment particles to form nanoporous composites. The attained composite properties like porosity, surface smoothness, mechanical properties and density properties depended strongly on the raw materials used. In general, higher kaolin content (~80 wt-%) led to controllable shrinkage during drying, which resulted in improved dimensional stability of composites, compared to a lower kaolin content (~50 wt-%). On the other hand, the use of a plasticizer and a high amount of CNF/CMF was essential to produce adequate elasticity for the composites. The performance of transistors when fabricated on the nanoporous composites was strongly dependent on the raw materials used. The formation of the semiconductor layer was affected by the porosity, roughness, hydrophobicity, polarity and absorption properties of the top-most layer at the composite. The developed natural fiber-based substrates may be applied to novel value-added applications in intelligent products, such as sensors and simple displays.

Keywords:

cellulose nano- and microfibrils (CNF / CMF), nanocellulose, kaolin pigment, printed electronics, transistors, composite, substrate

1. Introduction

The internet of things (IoT) is an emerging megatrend that connects physical devices, vehicles, and homes to the internet, allowing transmission, collection, and exchange of data between them [1]. IoT combines sensors, actuators, and electronics with network connectivity. For example, a biosensor combined with a modified atmosphere package (MAP) could detect a leakage of protection gas, instantly transmitting a warning via the integrated radio-frequency identification tags (RFID). Along the food supply chain, from warehouses, stores, and homes the leakage can be detected and reported immediately. This allows significant savings, *e.g.,* in food spoilage that is currently approximately 100 kg/capita/year in the western world [2]. The price of individual RFID tags is constantly decreasing allowing their wide-scale utilization in various applications. Recently, Delta Air Lines announced that they will integrate RFID tags to each individual checked-in baggage carried by the airline providing an accurate and real-time monitoring of the carried luggage [3]. These examples highlight the potential of IoT with interconnected devices: significant improvements in logistics and large economic benefits can be achieved. In order for it to be practical to integrate sensors into each individual package, a very low cost per unit is required (less than 0.01 USD/device). Functional printing is expected to play a key role in such cost-efficient production, as it allows a large number of devices to be manufactured in a roll-to-roll (R2R) process flow, resulting in a significant unit cost reduction.

In addition, sustainability has become an issue with conventional electronics. According to a research report by Gartner, smart phone sales exceeded 1 billion units in 2014 [4]. At the same time, the lifetime of electronics has become shorter resulting in large amounts of electronic waste. A more ecologically sustainable approach was suggested by Irimia-Vladu *et al.* [5] proposing replacing conventional inorganic components with organic counterparts. Printed electronics are traditionally manufactured on plastic films. However, a more ecologically sustainable alternative is to use renewable, recyclable, and biodegradable cellulose-based substrates [6-7]. An additional benefit of cellulose-based substrates is the possibility to control the ink setting properties, *e.g.,* by mineral pigment dispersion coating [8].

Hybrid materials combining CNF with pigments is an attractive field due to the CNF tendency to form strong and porous network structures in which inorganic particles can be homogeneously embedded [9]. Such flexible hybrid materials can be used for packaging applications, coatings, and film composites [10]. Moreover, flexible printed electronics and separation membranes can be obtained with further modification of hybrid composite structures [11]. There are numerous studies indicating that CNF/CMF films provide better smoothness and lower porosity of structure compared to traditional paper. The positive properties of CNF/ CMF films are approaching polymer plastic film properties [12-13].

The fabrication of low-cost pigment-cellulose nanofibril (PCNF) composite on a semi-pilot scale and its application as a separator substrate for printed supercapacitors has also been demonstrated [14]. Mineral pigment particles are traditionally widely used to improve gloss, smoothness, and printability of coated paper and paperboard grades. They can also be used to improve barrier properties and to obtain a lower porosity of hybrid films. High-strength CNF-talc hybrid barrier films were obtained by Liimatainen et al., in which the addition of platy talc particles resulted PCNF films with a small pore size and high oxygen barrier properties. An additional benefit of using mineral pigments is related to cost. They are much more cost effective compared to pure CNF solutions used in printed electronics. This means that minimizing the amount of CNF is the best solution considering the current price of CNF. [16].

CNF grades vary based on the raw materials and process treatments used. Here four different CNF grades were utilized ranging from enzymatic fibrillation to TEMPO-oxidation and lignocellulosic CNF (LCNF). Recent work [17] on lignocellulosic CNF on nanopapers obtained a significantly lowered porosity and water absorbency due to a small fraction of large pores. These findings suggest that lignin acts as an adhesive between fibrils, enabling improved mechanical properties. Lignin also decreases the surface energy of the fibrils, [18] reducing polarity and hydrophilicity of the CNFs. Here LCNF with kaolin pigments were combined.

The developed PCNF composites have a nanoporous pigment-fiber network structure that allows controlling of the ink absorption properties. Therefore, high-quality functional printing is possible on such smooth and nanoporous surfaces, without short circuit problems in the devices fabricated on the surface. The required substrate porosity and smoothness properties strongly depend on the used printing method, ink, solvent, and device design, which are affected by absorption, surface charge and binding properties. These substrate properties can be controlled by the selection of the used raw materials, including mineral pigments, cellulose micro/nanofibrils, and other additives.

This paper is organized as follows: in Section 2 describes the methods used for manufacturing and characterization of the kaolin-CNF composites. An ion-modulated transistor was deposited on the PCNF substrates with varying pigments and CNF constituents. Section 3 discusses the physicochemical characterization of the fabricated PCNF composite substrates and the performance of the deposited transistors. Finally, in Section 4 the conclusions of the present work are presented.

2. Experimental: Materials and Methods

2.1. Materials for composites

The TEMPO-oxidized cellulose nanofibrils (TCNF) were made from never dried, bleached softwood kraft pulp. The carboxylic acid content was 1 mmol/g of pulp. The fibers were fibrillated within a two-pass treatment by using a Microfluidizer M7115-30. The initial material for native (CNF) cellulose nanofibrils and high consistency enzymatic grades (ECMF) of cellulose microfibrils was never dried bleached softwood kraft pulp. For lignocellulosic grade nanofibrils (LCNF), the initial material was never dried, unbleached softwood kraft pulp. The fibril cellulose gels (CNF and LCNF grades) were obtained after six passes through a Masuko Sangyo (Supermasscolloider type MKZA10-15J) grinder by using a decreasing gap width and increasing operating power. The power varied from 1.7 to 2.5 kW. Rotation speed was fixed at 1500 RPM.

High-consistency enzymatic fibrillation of cellulose ECMF grade was processed at high consistency (20– 30% dry solids content during mixing). The procedure includes three key factors: mechanical low energy demand agitation, using of cellobiohydrolase (CBH) enzymes and temperature control of enzyme activity. A more detailed description of the manufacturing method can be found in [19].

The main pigment used in the study was the platy- shaped pigment kaolin Capim SP (Imerys Minerals Ltd, UK). The solids content of the slurry was 70 % and average particle size D_{50} was 0.54 µm. Another used grade was hyper-platy crystal kaolin HX spray-dried Barrisurf™ (Imerys Minerals Ltd, UK) with an especially high high aspect ratio of fine mineral particle size. The Barrisurf™ contains nano-dimensional thickness crystals. No additional dispersants were used. The plasticizer used in the study was D-Sorbitol (S1876, Sigma Aldrich).

2.2. Characterization of cellulose nanofibrils

Viscosity and degree of polymerization (DP) of initial raw materials were measured according to the standard ISO 5351 [20]. The cellulose nanofibrils were characterized using microscopy and UV-Vis spectroscopy as described in [20]. Congo Red (0.5%) and Toluidine Blue (0.1%) were used as marker colors in the optical microscopy characterization.

Rheological properties (storage modulus, loss modulus and shear viscosity) were measured at 0.5% consistency and at a temperature of 23 °C using a rotational rheometry (Anton Paar MCR301, ST22.4V vane spindle method) [21]. The charge of cellulosic gels was measured according to the standard SCAN-CM 65:02.]. Water retention of the cellulose nanofibrils (ÅAGWR) was measured based on the modified SCAN-C 62:00 method described in [22].

The grinder was connected to a frequency converter where the power of the grinder's motor was monitored. Specific energy consumption (SEC, kWh/kg) was calculated from the equation

$$E = \frac{P * t}{m} \quad , \qquad (1)$$

where P = gross power (kW), t = refining time (h), and m = mass of the pulp after refining (kg). The amount of residual fibers in the starting materials and mechanically treated samples was measured using the Kajaani Fiberlab Analyzer similar to Chinga-Carrasco *et al.* [23] and Mayer *et al.* [24]. Each sample was first soaked in 0.4 g/l consistency and dispersed using a high shear laboratory blender for 2–3 minutes. The samples were further mixed in 5 l of water at 40 mg/l consistency with an impeller for 10 minutes. 50 ml of the dispersed sample, or approximately 2 mg in dry weight, was pipetted into the analyzer, and fiber analysis was performed with two repeated measurements. The non-fibrillated fraction of fibers was thus estimated based on the amount of detected fibers and the concentration of the suspension.

2.3. Manufacturing of pigment-CNF (PCNF) composites

The nanoporous composites were formed by vacuum filtration. Cellulose micro / nanofibrils were first diluted to 0.5% dry solids content suspension in deionized water and stirred with an IKA Ultra Turrax T18 basic or a NETZSCH Shearmaster for 15 minutes at room temperature. The pigment suspension was prepared by mixing to 18–20% dry solids content. The pigment-CNF (PCNF) suspension was further diluted to a filtration concentration of 0.2% and mixed with a magnetic stirrer. The PCNF suspension was poured slowly into an over-pressurized sintered glass funnel filtration device and drainage was carried out at 0.8 bar. The sintered glass funnel device was equipped with a Whatman blue stripe filter paper with a porosity of 10–16 µm, in order to retain the fibrils and pigments and remove water.

The composites obtained after filtering were first pressed gently according to the procedure shown in Figure 1. The initial pressing was done with a 10 kg metal couch roll over the trial points ten times. The filtrated composites were sandwiched between filter papers, blotting papers and flat glass plates. The composites were directly extracted from the filtering paper or pre-dried with a contact dryer (62 °C) about three minutes and extracted after that. The required pre-treatment method was dependent on the CNF grade used.

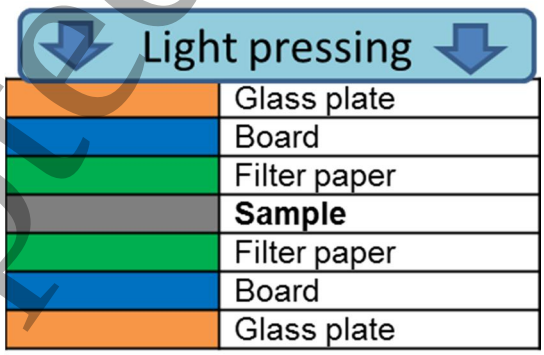

Figure 1. A schematic diagram of the pressing procedure of composite samples after vacuum filtration. The pressing was done using a metal roller. The role of the filter paper was to smoothen the surface of samples and the board acted as a soaking material for the excess water. The glass plate was needed as a rigid material in the pressing section.

The drying of the substrates was carried out using a contact dryer, *i.e.* a simultaneous application of both heat and pressure as described in [25]. The contact dryer included a curved metal plate, heated by electrical coils from the bottom side, and a tensioned dryer fabric. The experiments were carried out on a hot plate at 62°C for 15 minutes with a constant fabric tension of 2 kg/cm. After the drying process, the sheets were conditioned in a standard climate (25°C, 50% relative humidity (RH)) before calendering and physical testing. The sheets were calendered once using a laboratory scale calender with a hard roll nip, applying approximately 20 MPa pressure and 170 °C surface temperature on the lower roll. Composites with a target grammage of 100 g/m² were obtained and conditioned at 25°C and 50% RH prior to testing.

Scanning helium ion microscopy (HIM) provides high-resolution images, with a large depth of field on a wide range of materials, without sample damage. HIM gives information on topographic-, material-, crystallographic- and electrical properties of a sample. HIM can be directly used for high-resolution imaging of various non-conductive organic samples such as cellulose fibers without a need for a conductive carbon or metal coating. HIM can also be used for imaging the composites from macro- to nanoscale in order to complement observations from X-rays and optical coherence tomography.

PCNF trial points (Table 1) were imaged using HIM with beam current of 0.2–0.3 pA at 30 keV of energy. Three samples were prepared for each PCNF sample: top, bottom, and cross-section. The top and bottom sides were imaged with a 950 µm (the smallest possible magnification), 100 µm, 20 µm, and 4 µm field of view (FOV) at the same region on the sample. Small FOV images were not necessarily from the center of the larger FOV image, but a typical sample location was chosen. Sample charging was neutralized with an electron flood gun in all images with approximately 10 min of total collection time for each image. The original image resolution was 2048x2048 pixels. In this work the images have been compressed to half that resolution and image contrast has been enhanced (auto-leveling).

Table 1. Eight PCNF trial points.

Trial point	CNF	Pigment	Sorbitol [%]	CNF / pigment wt-%
CNF_20	CNF	Kaolin Capim SP	0	20/80
ECMF_43	ECMF	Kaolin Capim SP	15	42.5/42.5
ECMF_20	ECMF	Kaolin Capim SP	0	20/80
CNF_43	CNF	Kaolin Capim SP	15	42.5/42.5
LCNF_43	LCNF	Kaolin Capim SP	15	42.5/42.5
LCNF_20C	LCNF	Kaolin Capim SP	0	20/80
TCNF_20	TCNF	Kaolin Capim SP	0	20/80
LCNF_20B	LCNF	Barrisurf	0	20/80

2.4. Mechanical and structural testing of composites

The sheet grammage was analyzed by scanning the composite surface area using an Epson Perfection 3200 PHOTO scanner, whereas the thickness and density were determined with a Lorenzen & Wettre micrometer (SCAN-P 7:75). The air permeability was measured using a Lorentzen & Wettre SE 166 device based on the SCAN P-26:78 standard. The surface roughness was measured using an Altisurf 500 profilometer (Cotec, Évian, France) with a sampling resolution of 1 µm and a total measured area of 0.5 × 0.5 mm². The results were filtered with a Gaussian 0.1 mm sized screen. The surface roughness R_a was defined as:

$$Ra = \frac{1}{NM}\sum_{x=0}^{N-1}\sum_{y=0}^{M-1}\left|z_{x,y}\right| \quad (2)$$

where $z_{x,y}$ is the distance between the surface point and the mean surface height. The measurement was repeated six times for each measured sample.

The formation was measured utilizing a β-ray method [26]. In the VTT measurement system a storage phosphor screen (SPS) is exposed, through a complete sample, by beta radiation. Carbon 14 was used as the source of the radiation. The screen was scanned with a Fuji BAS-1800 II SPS reader (resolution of 0.1 mm) in order to determine the radiation absorption map, which was then converted to a grammage map. The standard deviation of grammage (*i.e.* formation) was then calculated using a measured area of 100 × 100 mm^2. The specific formation (unit $\frac{\sqrt{g}}{m}$) has been systematically used to include the effect of basis weight variation on the formation, obtained by dividing the standard deviation of basis weight by the square root of the basis weight.

The stain length test was performed using an IGT printability tester according to the AIC2-5T2000 standard and the Global Standard Tester instructions. The printing disc and a paper strip were placed on the sector of an IGT-printability tester and a drop of oil with a volume of 5.8 ± 0.3 mg was spread onto a stain in the printing nip. The length of the stain was measured.

Mechanical properties of the composite films were characterized using an Instron 8872 equipped with a 10 kN load cell. Dog-bone specimens of 30 mm gauge length and 4 mm width (see Figure 6) were cut from each film. Stress-strain data were produced using a strain rate of 1 mm/min, under controlled air conditions at 23°C and 50% RH, and the results are reported with standard deviation from ten parallel measurements.

2.4. Manufacturing and electrical performance of transistors

The used semiconductor layer consists of a blend of poly(3-hexyl thiophene) and the environmentally friendly and biodegradable insulating polymer poly(L-lactic acid) (P3HT:PLLA). Figure 2 shows a schematic of the device structure. The weight ratio used for the P3HT:PLLA blend was 1:4. The main reason for using this blend, instead of a pure semiconductor, was to achieve a thin semiconductor layer on top of the insulating layer (PLLA), even on a rough and absorptive substrate such as paper. The used solid electrolyte was a mixture of D-sorbitol and Choline Chloride (ChoCl) in high molecular weight polyolefin dispersion (HYPOD™ 8501, Dow Chemicals). Sorbitol and ChoCl were mixed at a molar ratio of 1:1 until the mixture turned into a liquid gel. This gel was then mixed with the water-dispersed binder. The electrolyte was finally spin casted at 3 000 RPMs for 30 s. The water evaporates during the casting process resulting in a solid film containing roughly 50 % sorbitol/ChoCl and 50% binder. The source-, drain-, and gate electrodes were all thermally evaporated at a pressure of approximately 10 mbar. Further details on the transistor fabrication processes and electronic properties of the reference ÅA transistor can be found from our previous publications [6, 27-29]. All transistor devices were fabricated and measured in a nitrogen atmosphere.

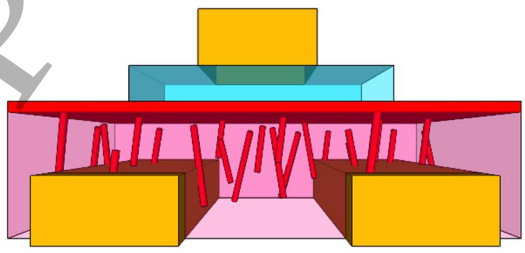

Figure 2. A schematic view of the device structure. The transistor electrodes have been drawn in orange, the solid electrolyte in blue, the semiconductor in red and the polymer insulator in pink.

The transistors were characterized by measuring transfer curves in saturation mode, where the drain voltage (V_D) was kept at -1 V and the gate voltage (V_G) was swept from 0 V to -1.2 V and back to 0 V. In Figure 8, a schematic of the transistor is shown. The figures of merit (FOMs) were extracted from the measured transfer curves. These include the drain current (I_D) measured at V_G = -1.2 V (ON-current), I_D measured at the point where V_G starts to increase logarithmically (OFF-current), the ratio between the ON- and OFF-current (ON/OFF-ratio), the gate current at V_G = -1.2 V (leakage) and the ratio between the leakage current and the ON-current (leakage/ON-current).

3. Results and discussion

Four different CNF grades were tested in this study: native CNF (CNF), lignocellulosic CNF (LCNF), TEMPO-oxidized CNF (TCNF) and enzymatic processed CMF (ECMF) together with kaolin clay pigment particles. Each of these raw material combinations resulted in different composite properties, *i.e.* surface roughness, mechanical properties, formation and density. Such characteristics were expected to have an effect on the deposited transistor properties as a proof-of-concept application example.

3.1. Physical properties of CNF grades

The characteristics of different CNF / CMFs are presented in Table 2. ÅAGWR values simulate different water removal mechanisms. Hence, they also correlate with the degree of fibrillation and the network structure. The water retention values of the fibrillated samples showed significant differences, with lower values, indicating better dewatering. Based on the water retention values, and also duration of the filtration during composite manufacturing, the TCNF grade had a higher capability to retain water and thus many times longer dewatering time. In addition, the LCNF grade had higher retention values than CNF- and ECMF grades. However, no clear effect was observed between composites of CNF-, LCNF- and ECMF grades in filtration times.

Table 2. Characterization of cellulose nanofibril materials.

Character	Unit	LCNF	CNF	TCNF	ECMF
Pulp		Unbleached kraft	Bleached kraft	Tempo SW pulp	Bleached kraft
Charge	mmol/g	0.07	0.02	1	0.02
Fibrillation Method		Grinding	Grinding	Microfluidization	Enzymatic
DP	SCAN	2087	1430	286	833
Transmittance, 800 nm	%	28	26	74	4
pH	pH	8.8	6.3	7.5	5.3
Consistency	%	1.75	1.76	1.16	18.56
Conductivity	µS/cm	403	116	794	51
Residual fibers	Fibers/mg	3272	2699	341	48105
Storage Modulus	Pa	37.5	14.8	56.8	0.02
Loss Modulus	Pa	5.8	2.2	7.3	0.3
Shear viscosity, 10 1/s	Pa·s	0.98	0.43	4.39	0.002
ÅAGWR, 30 sec.	g/g	297	233	446	229
SEC	kWh/kg	15.7	16	12	0.6

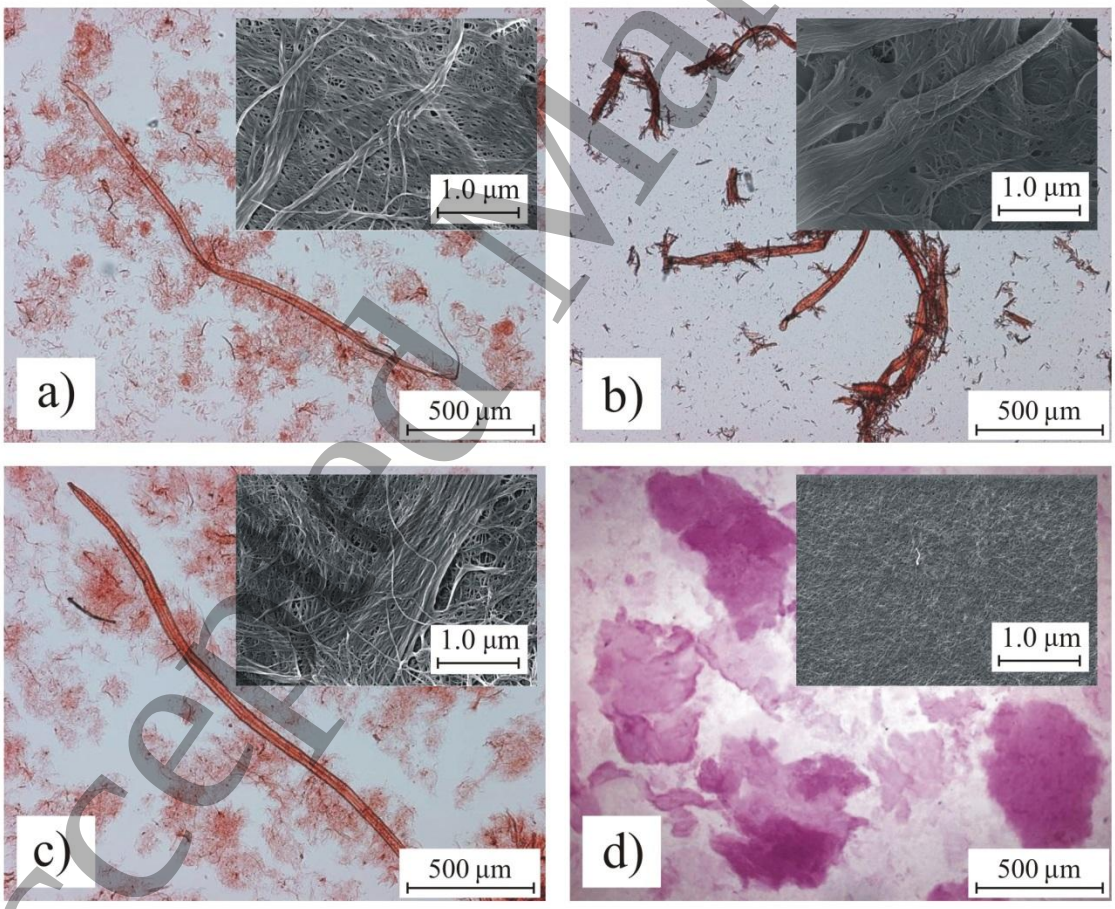

Figure 3. Microscopy and SEM images of different grades of cellulose nanofibrils a) CNF b) ECMF c) LCNF d) TCNF.

Optical microscopy images of the fibrillated nanomaterials are shown in Figure 3. The images show a great variation in sample appearance. The finest material observed was TCNF grade (D), not containing any fiber fragments or unfibrillated material. The CNF (A) and LCNF (C) grades had some intact fibers, but also a significant amount of fibrillated material, both as fibrils and fibril bundles. The ECMF (B) grade included a significant amount of microscale fibrils and also intact fibers. It had less fine material compared to the other grades and a low aspect ratio of particles. In summary, these observations correlate to the composite properties, *i.e.* the ECMF grade, together with pigments, produced a rougher surface with lower strength properties.

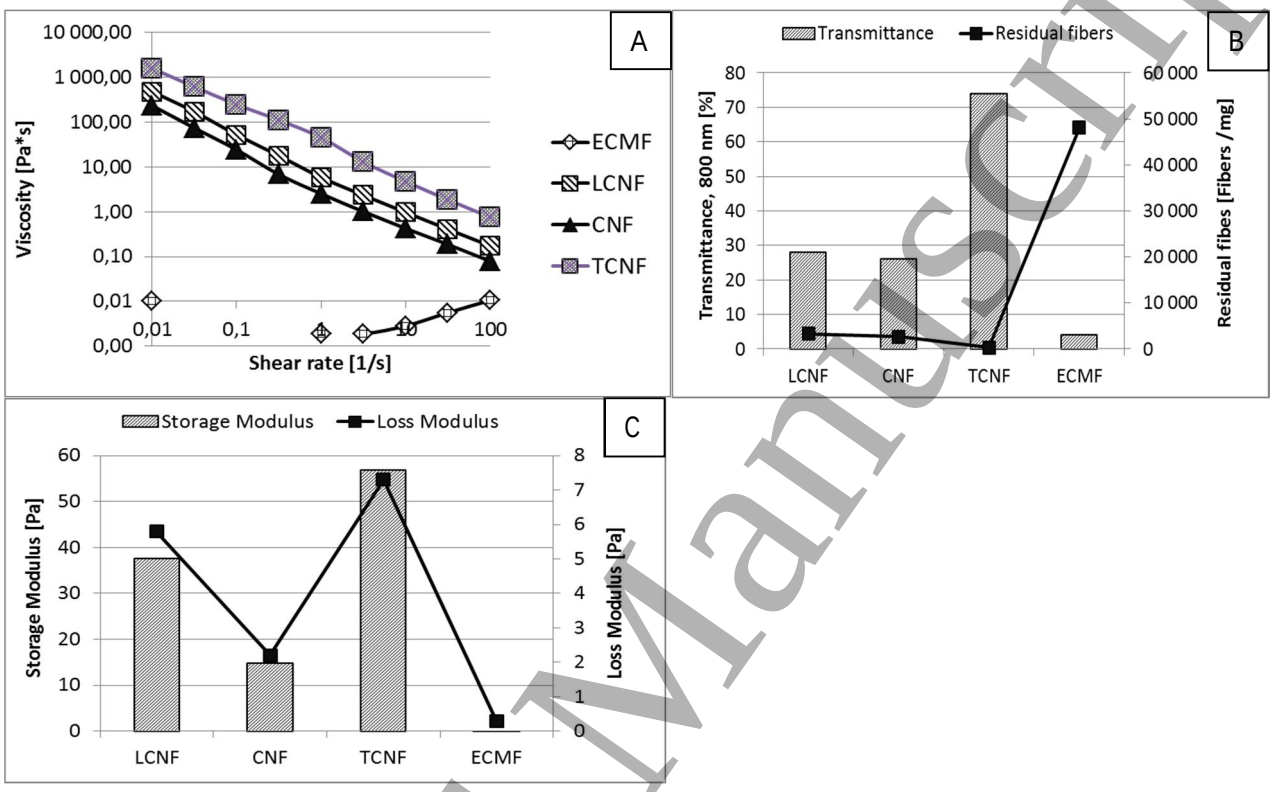

Figure 4. A viscosity curve as a function of the shear rate (A), transmittance and residual fibers (B), and the storage and loss modulus (C) of the CNF grades.

The degree of fibrillation for ECMF grade was clearly lower compared to the other grades as observed in Figure 4(B) resulting in a low shear viscosity (Figure 4A) and a high amount of residual fibers (Figure 4B). In addition, the ECMF grade was not a gel-like structure at 0.5% consistency and therefore thixotrophic behavior was not observed (Figure 4A). Correspondingly, the transmittance of the ECMF material was also at a significantly lower level (4 %-unit) compared to the other grades, with transmittances from 26 % to 74 % (Figure 4B). Furthermore, a low degree of fibrillation and aspect ratio of particles were observed to have an effect on other relevant composite properties. All these measured parameters explain why ECMF grades together with pigment particles resulted in a high surface roughness, low density, short stain length and insufficient mechanical properties of composites.

The TCNF grade, processed through the microfluidizer, had the highest transmittance values and the lowest amount of residual fibers, compared to the other grades, as presented in Figure 4B. Also, the shear viscosity of the TCNF gel was the highest (Figure 3A). Thus, it can be concluded, that the TCNF gel had the highest degree of fibrillation compared to the other grades. This is also supported by the light microscopy images (Figure 3). The high degree of fibrillation resulted in a significantly stronger gel structure compared to the other CNF grades measured with gel mechanical parameters: storage and loss modulus (Figure 3C). According to both storage and loss modulus the strongest gel was produced by the TCNF grade. A high loss modulus means a higher yield stress and usually high water retention behavior. LCNF also had a

significantly higher storage and loss modulus compared to the CNF grade, which was produced in a similar way from the same raw material. However, the bleaching process was only included in the production of the CNF grade. Therefore, it can be concluded that the presence of lignin resulted in a stronger gel. However, it is worth emphasizing that a stronger gel was not automatically followed with stronger mechanical composite properties in the presence of pigment particles. Together with the plasticizer, the LCNF grade resulted in having the highest tensile index, strain at break, and toughness. The difference from native grade was quite small, yet noticeable. In summary, more data is needed to study the CNF parameters' effects on the mechanical properties of the composites in future work.

3.2. Physical properties of PCNF composites

Composites made by vacuum filtration turned out to have a higher surface roughness on the bottom side than on the top side due to the effect of filtration paper, as observed also in earlier studies [30]. Therefore, an uneven cross-sectional structure was observed as shown in Figure 5A. The upper side was denser compared to the bottom side due to the higher amount of pigment particles on top. On the other hand, the bottom side included more cellulosic nanomaterial resulting in a higher porosity. The PCNF was filtrated from the bottom side of the composite during the forming process. Based on these observations, the upper side of the composite was selected as the surface upon which structural analysis and transistor fabrication would be carried out. In general, a migration path through the structure depends on particle packaging, alignment and various other factors. The long migration path suggests better barrier properties. In this work, Figure 5B displays the tortuous path with platy kaolin Barrisurf pigments (shape factor 100) which creates a long migration path through the composite.

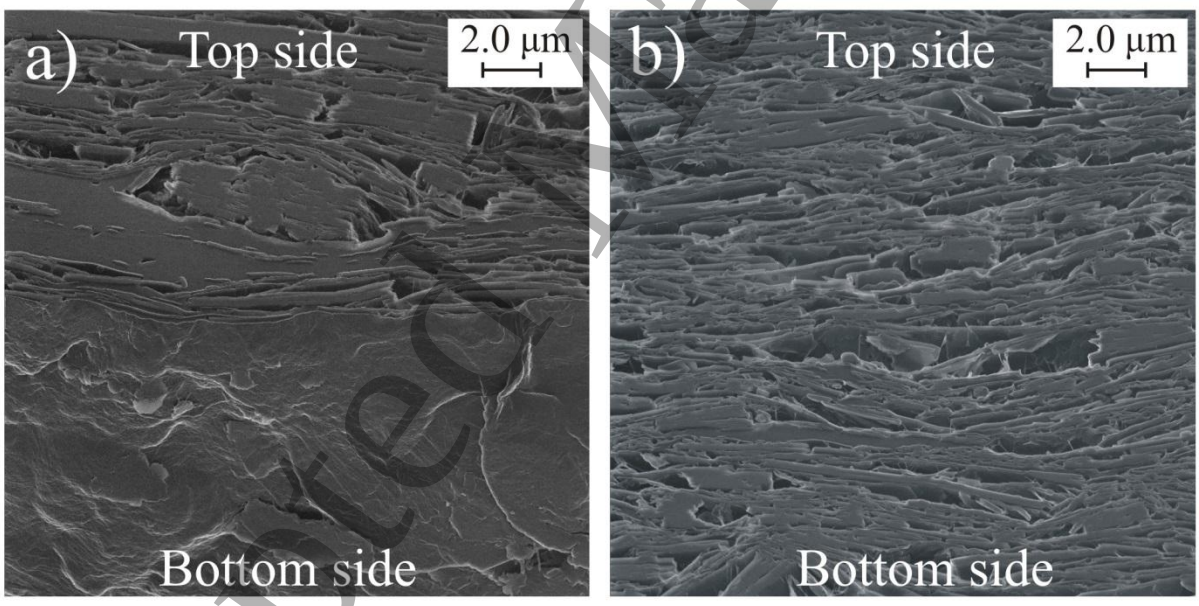

Figure 5. Cross-sections of composite LCNF_20B measured by HIM with a 20 µm field of view at a 45˚ angle relative to the cross-section surface resolution. The smooth cross-section was prepared using a broad ion beam cutting technique. The image a) shows both the original surface (lower half of the image) and the cross-section surface (upper half of the image) and in b) a tortuosity of the structure can be detected. The average porosity of the composite was approximately 20 %, based on a simple image analysis of the cross-sections.

A higher amount of cellulose nanomaterial in the composites (~43 wt-%) had a significant effect on the shrinkage during drying. The drying shrinkage leads to fragile and non-elastic film structures. In order to avoid this, sorbitol was added at 15 wt-% to the composites. It is noteworthy that composites made

without sorbitol as a plasticizer and higher amount of cellulosic nanomaterial were not included in this study due to the wrinkling and cockling of samples during the drying process. The dewatering behavior of the composites was considered to be an indicator that the composites could be suitable for large-scale mass production. Overall, a higher kaolin amount (80 %) improved the dimensional stability of the composites with controllable shrinkage during drying, compared to a lower amount (50 %).

The different composite surfaces were characterized using HIM. Significant differences were observed when varying the type of CNF used as seen in Figure 6. A higher roughness was attained with ECMF, compared to other grades, easily observable from images in Figures 6A-C. The high-resolution HIM images also reveal that the formed composites consist of individual fibrils and fibril networks that are binding the pigment particles together (Figures 6D-F). Especially the LCNF grade seems to produce film-like nanostructures on the surfaces of pigments.

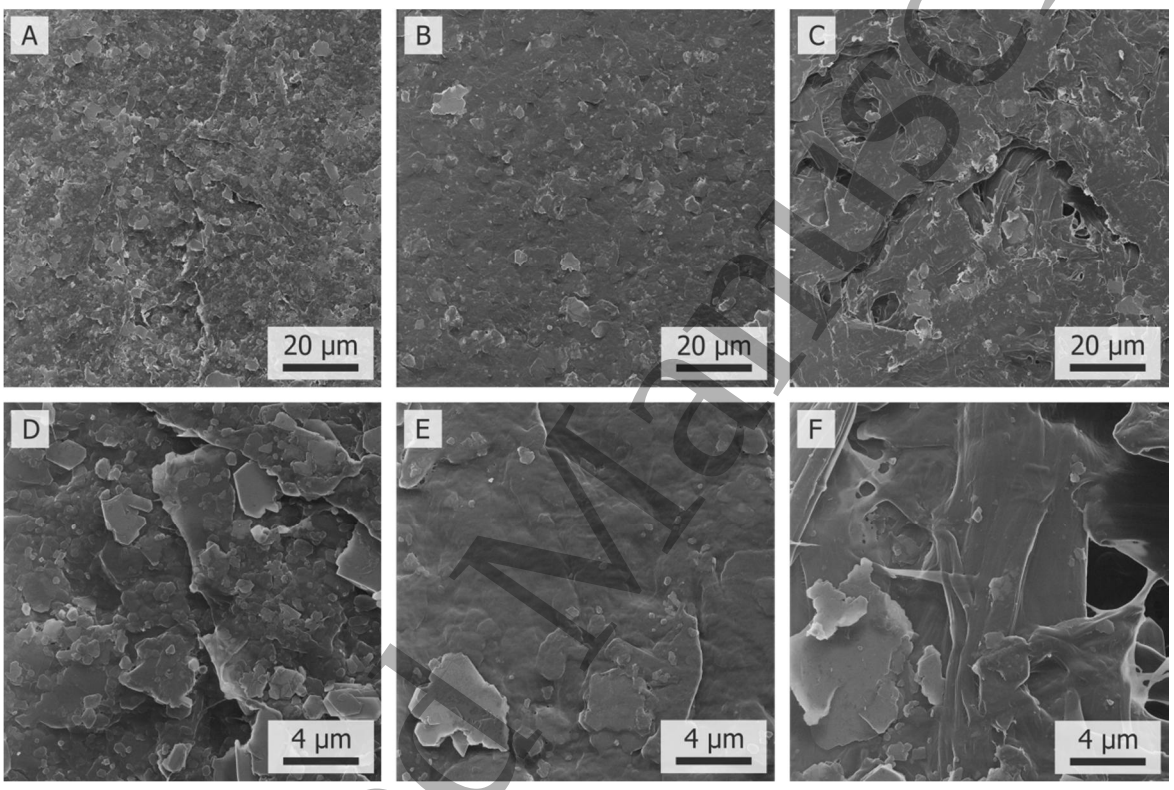

Figure 6. Helium Ion Microscope (HIM) images of composite surface morphology. The top side of the composites was imaged, using 100 µm (A-C) and 20 µm (D-F) fields of view. In A) and D) TCNF_20, in B) and E) LCNF_20C, and in C) and F) ECMF_20 are shown.

The density data is shown in Table 3 for the PCNF composites. The lowest material densities were achieved when ECMF grade (ECMF_43) and Barrisurf (LCNF_20B) were used as raw materials. The achieved low density for the ECMF grade is due to a lower amount of fibrillated material, when compared to the other CNF grades studied. As expected, the low density achieved when using Barrisurf is due to a higher aspect ratio of pigment particles resulting in an increased pore volume and surface roughness in the composite. The measured air permeability was below measurement limit for all trial points, which indicates a low porosity and good barrier properties.

Table 3. Composite properties, including grammage, thickness, density, formation, roughness and stain length for the produced composites, have been tabled. The strain length for the ÅA substrate was measured to be 150 mm.

Trial point	Grammage [g/m²]	Thickness [µm]	Density [kg/m³]	Formation Spec	Roughness Ra [µm]	Stain length [mm]
CNF_20	88.2 ± 2.2	58 ± 3	1522 ± 50	0.74	0.37 ± 0.02	138
ECMF_43	100.0 ± 7.7	75 ± 5	1332 ± 78	0.78	2.23 ± 0.55	54
ECMF_20	108.7 ± 2.5	76 ± 3	1427 ± 21	0.76	1.96 ± 0.27	-
CNF_43	112.6 ± 2.7	71 ± 1	1597 ± 28	-	0.54 ± 0.07	144
LCNF_43	102.1 ± 1.6	66 ± 1	1551 ± 19	-	0.67 ± 0.06	170
LCNF_20C	114.3 ± 2.5	76 ± 2	1512 ± 43	0.66	0.39 ± 0.04	159
TCNF_20	116.5 ± 1.5	76 ± 4	1531 ± 90	0.43	0.41 ± 0.06	138
LCNF_20B	111.6 ± 9.5	86 ± 7	1306 ± 101	0.59	0.74 ± 0.19	121

Surface smoothness is a crucial property for the composites when using them as a substrate for printed electronics. The lowest roughness values were measured for composites consisting of 80 wt-% Capim kaolin and 20 wt-% CNF or LCNF grade, however the results of the statistical analysis indicate that the TCNF grade reached the same smoothness values. On the other hand, the ECMF grade with the same pigment type and amount produced the lowest smoothness values. Therefore, the used CNF grade had a significant effect on surface smoothness. The rough ECMF grade resulted in the lowest surface smoothness, which is logical. However, the use of a finer TCNF grade did not improve the surface smoothness, compared to the CNF or LCNF grades. One explanation may be that on this particular roughness scale, the size and the shape of the pigment begins to dominate. Table 3 also shows the formation Spec-numbers. The most even formation was obtained with TCNF due to the low amount of residual fibers and thus a homogenous size distribution. This leads to a high degree of fibrillation and an increase of the bonding area for cellulose nanofibril pigment.

We can observe a correlation between the surface smoothness and the stain length if the scale is wide enough. Hence, a print penetration test can be used to estimate surface porosity. A low surface porosity leads to a longer stain length in the stain test. Correspondingly, a high surface porosity leads to a shorter stain length with a higher absorbance of the used solvent into the structure. The correlation between stain length and Hg-porosity measurement is good based on earlier studies [31].

3.3. Strength properties of PCNF composites

Figure 7 summarizes the measured mechanical properties of the PCNF composites. The use of a plasticizer in the PCNF composites clearly increased both the strain at break and the toughness for trial points CNF_43 (native grade) and LCNF_43 (LCNF grade), which are in good agreement with values in the literature [16]. A different behavior was observed for the ECMF_43, most probably due to its poor ability to bind pigments together. This is due to a low degree of fibrillation of ECMF fibers, which can be seen in the CNF characterization data, *i.e.* a high amount of residual fibers and a lower shear viscosity. Also, the low pH level of ECMF grade will have an impact on the interactions of kaolin and fibrils causing flocculation and this should be taken account in future studies [32]. On the other hand, the use of a plasticizer and a higher amount of CNF was essential to produce adequate elasticity for the composites. Without using a plasticizer, both strain at break and toughness values of composites were insufficient for further converting processes.

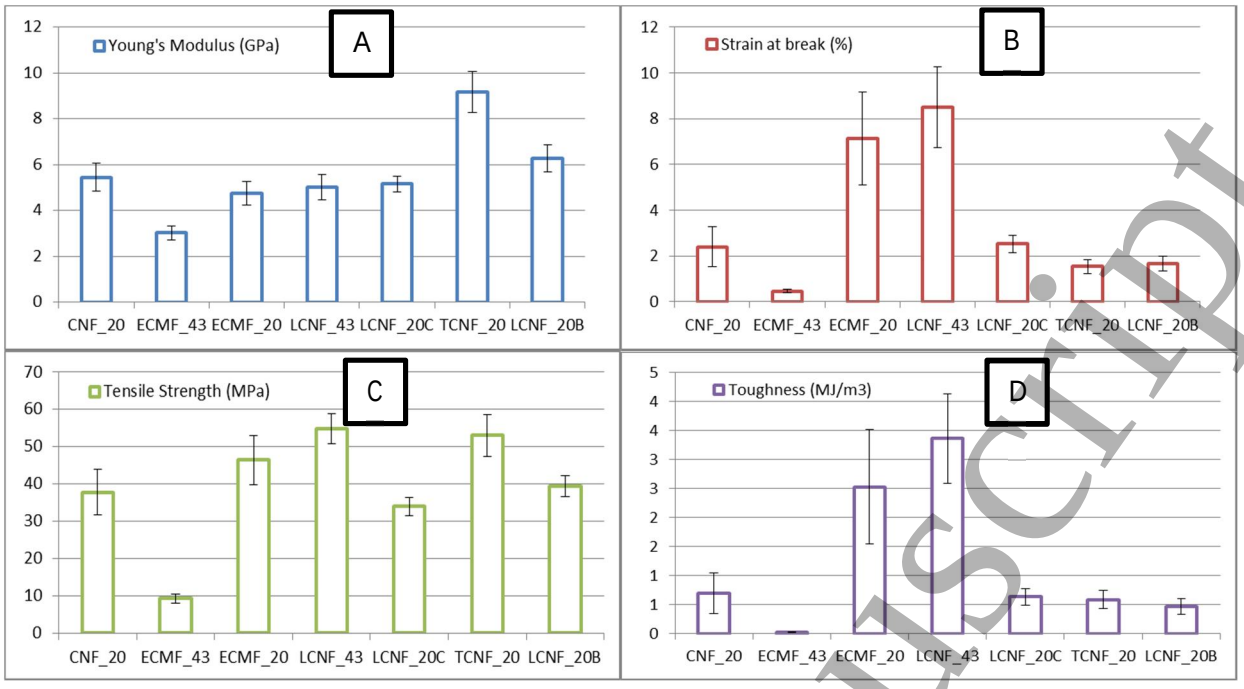

Figure 7. Mechanical properties of the composites for the studied trial points A) Young's Modulus [GPa] B) Strain at break [%]C) Tensile Strength [MPa] and D)Toughness [MJ/m³].

The use of TCNF grade produced composites with the highest Young's modulus. Additionally, the trial point with 80 wt% pigment loading together with TCNF produced composites with a high tensile strength. Comparing the trial points LCNF_20C and LCNF_20B, where the only difference was the pigment used, it can be concluded that Barrisurf produced a slightly higher tensile strength and Young's modulus, compared to Capim SP mineral. This is probably due to the high aspect ratio of particles in Barrisurf pigment. PCNF composites with the best mechanical properties were produced using LCNF grade together with a plasticizer (LCNF_43), resulting in the composites having a high tensile strength, strain at break and toughness, and also an adequate Young's modulus value.

3.4. Transistor functionality on PCNF composites

Figure 2 shows the schematic of the model transistor device and Figure 8 shows two examples of transfer curves (TCNF_20 and ÅA). Table 4 summarizes the FOM values that were extracted from the measured transfer curves. No clear difference in the film forming properties of the semiconductor layer can be distinguished from the appearance of the devices. Typically, during the casting of this particular semiconductor, it will show different colors depending on semiconductor crystallinity and thickness. The composite substrates themselves have slightly different brightness.

Table 4 shows that the trial points CNF_43, LCNF_43 and LCNF_20B have similar transistor properties compared to that of the reference ÅA paper. They have slightly lower ON-currents and higher leakage currents, but are still comparable to the ÅA reference device. The PCNF composites can thus be used as a natural fiber-based substrate for electronic devices without any significant loss of performance. Trial point TCNF_20 showed the highest ON/OFF-ratio, but it also showed the highest leakage current. This would result in increased power consumption and would not be a desirable alternative for the ÅA paper. Trial points CNF_20 and LCNF_20C showed poor transistor characteristics, while ECMF_43 showed no transistor characteristics at all. No transistors were fabricated on the ECMF_20 due to high roughness values that would have resulted in similar poor transistor performance as in the case of ECMF_43.

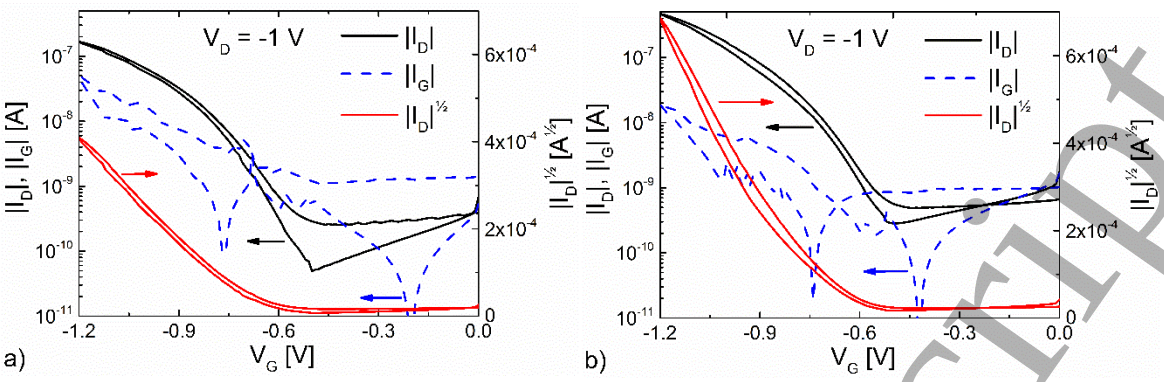

Figure 8. Transfer curves of transistors fabricated on a) composite TCNF_20 and b) ÅA reference. The black curves represent the I_D in saturation mode during gate sweeps between 0 V and -1.2 V, the red curve is the square root of I_D and the dashed curve is the I_G.

Table 4. FOMs, calculated using the transfer curves of the same transistor model, fabricated on different substrates. Trial point ECMF_43 did not show transistor characteristics and therefore corresponding FOMs could not be calculated. A multilayer paper from Åbo Akademi was used as a reference [33]. All units are in amperes, except for the ratios that are unitless.

Trial point	ON-current [E-07 A]	OFF-current [E-10 A]	ON/OFF-ratio	Leakage [E-08 A]	Leakage/ON-current
CNF_20	1.4	9.1	150	14	1.01
ECMF_43	-	-	-	-	-
CNF_43	3.0	2.1	1460	4.0	0.13
LCNF_43	2.8	2.1	1370	3.3	0.12
LCNF_20C	0.3	10	30	0.4	0.13
TCNF_20	1.7	0.5	3460	5.0	0.29
LCNF_20B	3.9	2.5	1570	3.0	0.08
ÅA	4.7	2.9	1650	2.0	0.04

Conclusions

Important properties of composites for printed electronics applications include surface smoothness, nanoscale porosity, and controlled barrier properties. A nanoporous pigment-fiber network structure allows optimized absorption of ink solvents into the substrate. Additionally, such optimized structure allows high-quality printing and manufacturing of functional devices on smooth and closed surfaces. In this study four different CNF/CMF grades were utilized together with kaolin clay pigment particles. Each of the raw material combinations resulted in different composite properties, *e.g.* surface roughness, mechanical properties, formation, and density. Ground lignocellulosic nanofibrils (LCNF), together with a plasticizer and kaolin pigment particles, resulted in the films having high mechanical strengths without impairing water removal during the manufacturing process. TEMPO oxidized cellulose nanofibrils (TCNF) with kaolin particles formed stiff and even surfaces but had poor dewatering properties due to high fibrillation level of the TCNF. The use of a plasticizer and a high amount of CNF/CMF was essential to produce adequate elasticity in the composites.

The CNF/CMF grade plays a significant role in surface smoothness and porosity of composites. Such characteristics have a clear effect on the properties of, e.g. transistors fabricated on said composite

substrates. Furthermore, the low degree of fibrillation and the aspect ratio of particles were observed to have a weakening effect on relevant properties of composites. Several of the studied PCNF composite types had similar transistor properties compared to that of a reference paper designed for printed electronics. The PCNF composites have slightly lower ON-currents and higher leakage currents. However, they are still comparable and these PCNF composites can be used as a natural fiber-based substrate for transistor devices, without any significant loss of device performance.

Acknowledgements

Special thanks to VTT colleagues Merja Selenius for composite tests, Vesa Kunnari for plasticizer material and Jaakko Pere for providing ECMF material. One of the authors (JJS) wishes to acknowledge financial support by the Academy of Finland (grant no. 250 122, 256 263, 283 054 and 269973) and author KA acknowledges funding from the Finnish Centre of Excellence on Nuclear and Accelerator Based Physics by Academy of Finland (grant no. 251 353). Jere Manni, from Top Analytica Ltd., is acknowledged for preparing a broad ion beam milled cross-sectional sample for HIM imaging.

References:

1. Greencard S: The Internet of Things, MIT Press, Cambridge, (2015).
2. Gustavsson J, Cederberg C, Sonesson U, van Otterdijk R, and Meybeck A: Global Food Losses and Food Waste. Food and Agriculture Organization of the United Nations (FAO) report, Rome, 2011.
3. Forbes: Why Delta Air Lines is less likely than its rivals to lose your bags, Aug 31st, (2016).
4. Gartner report: "Market Share: Devices, All Countries, 4Q14 Update." Gartner, (2014).
5. Irimia-Vladu M: ''Green'' electronics: biodegradable and biocompatible materials and devices for sustainable future, Chem. Soc. Rev. 43, 588-610 (2014).
6. Bollström R, Määttänen A, Tobjörk D, Ihalainen P, Kaihovirta N, Österbacka R, Peltonen J, and Toivakka M: A multilayer coated fiber-based substrate suitable for printed functionality, Org. Electron. 10, 1020-1023 (2009).
7. Tobjörk D and Österbacka R: Paper electronics, Adv. Mater. 23, 1935-1961 (2011).
8. Lehtinen E (ed.): Pigment Coating and Surface Sizing of Paper, FAPET, Jyväskylä, (2000).
9. Sehaqui, H., Zhou, Q., Ikkala, O., & Berglund, L. A. (2011). Strong and tough cellulose nanopaper with high specific surface area and porosity. Biomacromolecules, 12(10), 3638–3644. https://doi.org/10.1021/bm2008907
10. Aulin, C., Salazar-Alvarez, G., & Lindström, T. (2012). High strength, flexible and transparent nanofibrillated cellulose-nanoclay biohybrid films with tunable oxygen and water vapor permeability. Nanoscale, 4(20), 6622–8. https://doi.org/10.1039/c2nr31726e
11. Wei, H., Rodriguez, K., Renneckar, S., & Vikesland, P. J. (2014). Environmental science and engineering applications of nanocellulose-based nanocomposites. *Environ. Sci.: Nano*, *1*(4), 302–316. https://doi.org/10.1039/C4EN00059E
12. González, I., Alcalà, M., Chinga-Carrasco, G., Vilaseca, F., Boufi, S., & Mutjé, P. (2014). From paper to nanopaper: Evolution of mechanical and physical properties. Cellulose, 21(4), 2599–2609. https://doi.org/10.1007/s10570-014-0341-0
13. Syverud, K., & Stenius, P. (2009). Strength and barrier properties of MFC films. Cellulose, 16(1), 75–85. https://doi.org/10.1007/s10570-008-9244-2
14. Torvinen K, Lehtimäki S, Keränen JT, Sievänen J, Vartiainen J, Hellén E, Lupo D, and Tuukkanen S: Pigment-cellulose nanofibril composite and its application as a separator-substrate in printed supercapacitors, Electron. Mater. Lett. 11, 1040-1047 (2015).

15. Liimatainen H, Ezekiel N, Sliz R, Ohenoja K, Sirviö JA, Berglund L, Hormi O, and Niinimäki J: High-strength nanocellulose–talc hybrid barrier films, Appl. Mater. Interf. 5, 13412–13418 (2013).
16. Hoeng F., Denneulin A., and Bras J.:Use of nanocellulose in printed electronics: a review, Nanoscale, 2016,8, 13131-13154 DOI: 10.1039/c6nr03054h
17. Rojo E, Peresin MS, Sampson WW, Hoeger IC, Vartiainen J, Laine J, and Rohas OJ: Comprehensive elucidation of the effect of residual lignin on the physical, barrier, mechanical and surface properties of nanocellulose films, Green Chem. 17, 1853-1866 (2015).
18. Laine J, Stenius P, Carlsson G, and Ström G: Surface characterization of unbleached kraft pulps by means of ESCA, Cellulose 1, 145-160 (1994).
19. Kemppainen K., Hiltunen J. and Pere J. "Process for producing fibrillated cellulose material" WO2015/092146; Patent reference
20. Kangas, H., Lahtinen, P., Sneck, A., Saariaho A.-M., Laitinen O. and Hellén, E., (2014). Characterization of fibrillated celluloses. A short review and evaluation of characteristics with a combination of methods, Nordic Pulp & Paper Research Journal, 29(1), 129-143.
21. Lahtinen, P., Torvinen, K., Kangas, H., Liukkonen, S., Sneck, A., Peresin M. S., Pere, J., Hänninen, T., Meyer, V., and Tammelin, T. Effect of Fibrillated Cellulosic Additives on Paper Strength Properties. Proceedings from the PaperCon 2014, Nashville, TN, USA 27.-30.4.2014.
22. Lahtinen P., Liukkonen S., Pere J., Sneck A. and Kangas H. (2014), comparative study of fibrillated fibers from different mechanical and chemical pulps, BioResources 9(2) pp. 2115-2127
23. Chinga-Carrasco, G., Optical methods for the quantification of the fibrillation degree of bleached MFC materials, Micron 48 (2013) 42–48.
24. Mayer, V., Tapin-Lingua, S., Da Silva Perez, D., Arndt, T., and Kautto J., Technical opportunities and economic challenges to produce nanofibrillated cellulose in pilot-scale: NFC delivery for applications in demonstration trials. SUNPAP Final conference 19.6.2012.
25. Timofeev O., Torvinen K., Sievänen J., Kaljunen T., Kouko J. and Ketoja J.A., " Drying of Pigment-Cellulose Nanofibril Substrates" Materials 2014, 7, 6893-6907; doi:10.3390/ma7106893
26. Komppa, A., and Komppa, O. (1996): Measurement of paper formation, 50th Appita Annual General Conf, Auckland, New Zealand, pp. 803-808.
27. F. Pettersson, R. Österbacka, J. Koskela, A. Kilpelä, T. Remonen, Y. Zhang, S. Inkinen, C.-E. Wilén, R. Bollström, M. Toivakka, A. Määttänen, P. Ihalainen, and J. Peltonen, MRS Commun. 4, 51 (2014).
28. F. Pettersson, T. Remonen, D. Adekanye, Y. Zhang, C. Wilén, and R. Österbacka, ChemPhysChem 16, 1286 (2015)
29. F. Pettersson, D. Adekanye, and R. Österbacka, Phys. Status Solidi Appl. Mater. Sci. 212, 2696 (2015).
30. Penttilä A, Sievänen J, Torvinen K, Ojanperä K, Ketoja JA (2013) "Filler-nanocellulose substrate for printed electronics: experiments and model approach to structure and conductivity" Cellulose 20:1413-1424. doi: 10.1007/s10570-013-9883-9
31. Toivakka M. : "Future of paper as substrate for printed electronics and sensors", ISAB 2012 meeting http://www.funmat.fi/ISABmeeting2012/24%20-%20Toivakka%20-%20Future%20of%20paper%20as%20substrate%20for%20printed%20electronics%20and%20sensors.pdf
32. Addai-Mensah J. "Enhanced flocculation and dewatering of clay mineral dispersions", Powder Technology 179 (2007) 73-78
33. Bollström R. "Paper for printed electronics and functionality" Doctoral Thesis (2013) Åbo Akademi Finland http://urn.fi/URN:NBN:fi-fe201311077025